Modeling of Luneburg Lenses with the Use of Integral Equation Macromodels

Andrzej A. KUCHARSKI

Telecommunications and Teleinformatics Department, Wrocław University of Technology,
Wybrzeze Wyspianskiego 27, 50-370 Wrocław, Poland

andrzej.kucharski@pwr.wroc.pl

Abstract. *The so-called integral equation macromodel allowing to efficiently include Luneburg lens into the body-of-revolution method-of-moments (BoR-MoM) computational scheme is described. In the process of the macromodel construction, we make use of the equivalence-principle domain-decomposition-method (EP-DDM) and the asymptotic waveform evaluation (AWE) method. By the use of the macromodel, the number of unknowns in the final system of equations is reduced to those describing sources on the equivalent surface surrounding the lens. Moreover, thanks to the macromodel being valid in a certain frequency interval, the domain decomposition procedure does not have to be repeated for every frequency of interest, but it should only be done in some specified frequency points. However, the range of validity of the macromodel should be carefully investigated on the basis of full radiation pattern rather than on the basis of a single direction of observation.*

Keywords

Method of moments, macromodel, Luneburg lens.

1. Introduction

The Luneburg lens [1] is a well-know type of spherical dielectric lens with dielectric permittivity profile depending on the distance from the center, according to the formula:

$$\varepsilon_r(r) = 2 - \left(\frac{r}{a}\right)^2, \quad 0 \le r \le a, \qquad (1)$$

where r is the distance from the sphere center, a denotes the radius of the sphere.

In the optical regime, it possesses an interesting property of collimating rays originating from the point source placed at the lens surface, into parallel rays leaving the lens on its other side. Although this property does not transform fully into radio-frequency bands [2], the lens plays an important role in the design of antennas [3]. Although the interest in this technique has been abandoned for many years [4]
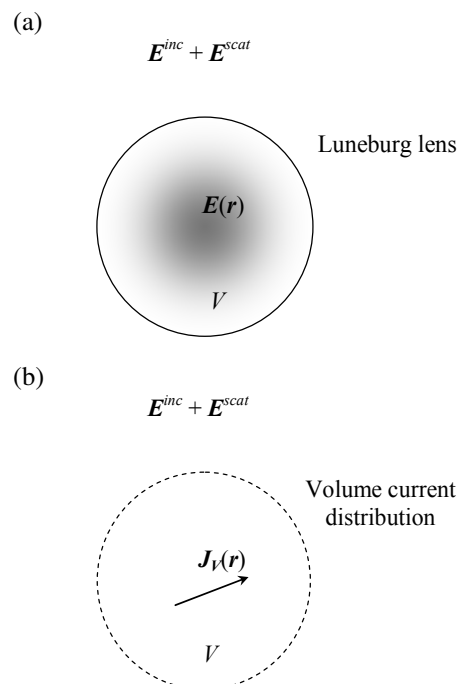
mainly due to problems with production of inhomogeneous dielectrics, it is recently re-awakened because of possible applications in future High Altitude Platform (HAP) systems. Those applications include obtaining the whole cellular pattern from the single platform [5], as well as the construction of ground-based antennas with mechanical scanning possibilities [6]. Modeling of antenna configurations incorporating Luneburg lenses provides some challenge for computational methods, as their inhomogeneous nature enforces either applying differential-equation/grid methods or using volume sources within integral-equation/method-of-moments (MoM) solutions. In the first case one has to either use proper absorbing conditions to model the radiation [2], or to use hybrid solution [7]. The second choice (MoM) leads to a large number of unknowns in the linear equation system, described by a dense matrix. In both cases, the situation is complicated by the fact that the lens is usually electrically large.

(a)

$E^{inc} + E^{scat}$

Luneburg lens

$E(r)$

V

(b)

$E^{inc} + E^{scat}$

Volume current distribution

$J_V(r)$

V

Fig. 1. Luneburg lens immersed in the incident field (a) and the equivalent situation (b).

Alternatively, one may apply solutions of Maxwell's equations for a concentric multishell dielectric sphere [3], [6], which is however outside the scope of this paper. The need for large computational resources may be relaxed, if we note that the lens possesses rotational symmetry. Thus, we may apply the well-known body-of-revolution (BoR) technique, in which solution scheme is decomposed into a number of azimuthal modes, analyzed separately (cf. [7–9]). For some excitations, like plane wave traveling along the BoR symmetry axis, it is even possible to limit the analysis to one mode, thus reducing the problem from three-dimensional to two-dimensional. Even if this is the case, the computation may require a relatively large number of unknowns [9], which makes it quite time-consuming to perform for instance wideband feed optimizations. Here, we give a simple solution to this problem, applying previously introduced technique of integral equation macromodels [10]. The idea used in this paper was initially given in [11] for wideband analysis of partially inhomogeneous bodies of revolution. However, examples given in [11] were confined to simple two-layered spheres. Here, we show its usefulness for more sophisticated case of Luneburg lenses. The main purpose of the paper is twofold: first, we show that it is really possible to describe the Luneburg lens as a wideband "black box" with the number of unknowns in the final equation set equal to that of a homogeneous object, second, we investigate carefully the "bandwidth" of the macromodel based on the full radiation pattern analysis.

Throughout the paper we assume $e^{j\omega t}$ time convention.

2. Integral Equation Macromodel Based on Volume-Surface Integral Equation

2.1 Classical Volume Integral Equation (VIE) Formulation

The original situation to be analyzed is depicted in Fig. 1. The usual procedure relies on replacing the dielectric by the volume distribution of polarization current, radiating in free-space [12], [13]:

$$\mathbf{J}_V(\mathbf{r}) = j\omega[\varepsilon(\mathbf{r}) - \varepsilon_0]\mathbf{E}(\mathbf{r}). \qquad (2)$$

Then we formulate the volume integral equation, which states that the total electric field in the body volume (as at any other point in space) is a sum of incident and scattered fields (cf. [13]):

$$\mathbf{E}^{inc}(\mathbf{r}) + \mathbf{E}^{scat}(\mathbf{r}) = \frac{\mathbf{J}_V(\mathbf{r})}{j\omega[\varepsilon(\mathbf{r}) - \varepsilon_0]}, \quad \mathbf{r} \in V. \qquad (3)$$

Above, vector $\mathbf{r}$ indicates the observation point. Electric field due to polarization current may be obtained from standard mixed-potential formula:
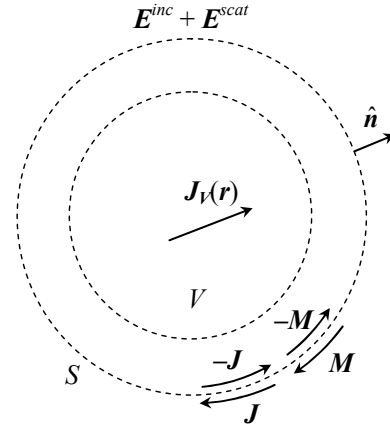

Fig. 2. Additional surface S with equivalent currents surrounding the lens (external and internal equivalent situations combined into the single picture).

$$\mathbf{E}^{scat}(\mathbf{r}) = \mathbf{E}^{scat}(\mathbf{J}_V) = -\frac{j\omega\mu_0}{4\pi}\int_V \mathbf{J}_V(\mathbf{r}')\frac{e^{-jk|\mathbf{r}-\mathbf{r}'|}}{|\mathbf{r}-\mathbf{r}'|}dV'$$
$$+ \frac{1}{4\pi\varepsilon_0}\nabla\int_V \frac{\nabla\cdot\mathbf{J}_V(\mathbf{r}')}{j\omega}\frac{e^{-jk|\mathbf{r}-\mathbf{r}'|}}{|\mathbf{r}-\mathbf{r}'|}dV' \quad (4)$$

where $\mathbf{r}'$ indicates source point, and $k = \omega\sqrt{\varepsilon_0\mu_0}$ is a wavenumber.

It is to be noted that, usually, it is the electric flux density used as the unknown quantity [13], which enables application of roof-top-like basis and testing functions in the method-of-moments (MoM) solution.

For bodies with rotational symmetry, the scheme proposed in [9] may be used to efficiently solve equation (3). The method utilizes conventional azimuthal mode decoupling together with specially constructed divergence-less basis functions. Sample results obtained with this basic approach will be shown in the next section as the comparison data.

2.2 Volume-Surface (VIE-SIE) Formulation and Domain Decomposition Method (DDM)

Another solution is to apply domain decomposition scheme based on the equivalence principle [14]. Thus, we surround the inhomogeneous part by the artificial surface S, which may or may not coincide with the outer surface of the analyzed body (Fig. 2). Then, introducing artificial electric and magnetic currents, and applying usual internal and external equivalent situations, we arrive at the system of equations [11], [15]:

$$\hat{\mathbf{n}} \times (\mathbf{E}^{inc} + \mathbf{E}_e^+(\mathbf{J}, \mathbf{M})) = \hat{\mathbf{n}} \times \mathbf{E}_i^-(-\mathbf{J}, -\mathbf{M}, \mathbf{J}_V) \quad \text{on } S, \ (5)$$

$$\hat{\mathbf{n}} \times (\mathbf{H}^{inc} + \mathbf{H}_e^+(\mathbf{J}, \mathbf{M})) = \hat{\mathbf{n}} \times \mathbf{H}_i^-(-\mathbf{J}, -\mathbf{M}, \mathbf{J}_V) \quad \text{on } S, \ (6)$$

$$\mathbf{E}_i = \mathbf{E}_i^-(-\mathbf{J}, -\mathbf{M}, \mathbf{J}_V) \quad \text{in } V. \qquad (7)$$

Above, sub-scripts e and i denote environments external and internal to S, respectively, while super-scripts "+" and "−" show that corresponding fields are calculated, as the observation point approaches S from outside and inside, respectively. Note that although in sub-sequent calculations, external and internal environments are assumed to be the same (free space), in general it may not be the case. For example, different Green's functions, accounting for other configurations, may be used for the outer environment. Note also that the above equations are the same as in the case of partially inhomogeneous dielectric bodies [16]. Obviously, fields in (5) – (7) produced by several currents are understood as superpositions of fields produced by individual currents.

Formulas to obtain fields due to surface electric current for the internal interactions are standard ones:

$$\mathbf{E}_i(\mathbf{r}) = \mathbf{E}_i(\mathbf{J}) = -\frac{j\omega\mu_0}{4\pi}\int_S \mathbf{J}(\mathbf{r}')\frac{e^{-jk|\mathbf{r}-\mathbf{r}'|}}{|\mathbf{r}-\mathbf{r}'|}dS'$$
$$+ \frac{1}{4\pi\varepsilon_0}\nabla\int_S \frac{\nabla\cdot\mathbf{J}(\mathbf{r}')}{j\omega}\frac{e^{-jk|\mathbf{r}-\mathbf{r}'|}}{|\mathbf{r}-\mathbf{r}'|}dS', \quad (8)$$

$$\mathbf{H}_i(\mathbf{r}) = \mathbf{H}_i(\mathbf{J}) = -\frac{1}{4\pi}\nabla\times\int_S \mathbf{J}(\mathbf{r}')\frac{e^{-jk|\mathbf{r}-\mathbf{r}'|}}{|\mathbf{r}-\mathbf{r}'|}dS', \quad (9)$$

while the formulas for fields due to magnetic currents may be easily obtained by duality, and fields due to the volume electric current are the counterparts of (8), (9), with integration over surface S replaced with integration over volume V. For external interactions, the situation depends on the environment, in which the lens (together with surrounding surface S, is immersed. If the medium is again the free space, obviously (8) and (9) are applied.

After application of MoM, the system (5) – (7) is transformed into the matrix equation:

$$\begin{bmatrix} \mathbf{Z}_{EJ}^{SSe}+\mathbf{Z}_{EJ}^{SSi} & \mathbf{Z}_{EM}^{SSe}+\mathbf{Z}_{EM}^{SSi} & \mathbf{Z}_{EJ}^{SVi} \\ \mathbf{Z}_{HJ}^{SSe}+\mathbf{Z}_{HJ}^{SSi} & \mathbf{Z}_{HM}^{SSe}+\mathbf{Z}_{HM}^{SSi} & \mathbf{Z}_{HJ}^{SVi} \\ \mathbf{Z}_{EJ}^{VSi} & \mathbf{Z}_{EM}^{VSi} & \mathbf{Z}_{EJ}^{VVi} \end{bmatrix}\begin{bmatrix} \mathbf{J} \\ \mathbf{M} \\ \mathbf{J}_V \end{bmatrix}=\begin{bmatrix} \mathbf{E}^{inc} \\ \mathbf{H}^{inc} \\ \mathbf{0} \end{bmatrix}$$
$$(10)$$

where $\mathbf{J}$, $\mathbf{M}$, $\mathbf{J}_V$ now denote vectors of coefficients describing approximations of respective currents. Similarly, $\mathbf{E}^{inc}$, $\mathbf{H}^{inc}$ are vectors resulting from testing of incident fields at S. $\mathbf{Z}_{PQ}^{KLr}$ denotes sub-matrix with elements corresponding to field P (electric E or magnetic H) from currents Q (electric J or magnetic M) flowing in the domain L (surface S or volume V) tested over domain K (also S or V), while the radiation takes place in the environment r (external e or internal i).

In the system, we obviously have more unknowns, than in the matrix counterpart of (3), because in addition to unknowns resulting from the volume current distribution, we have coefficients describing surface electric in magnetic currents. However, we can replace the set by [11]:

$$\left[\mathbf{Z}^{SSe}+\left\{\mathbf{Z}^{SSi}-\mathbf{Z}^{SVi}\left(\mathbf{Z}_{EJ}^{VVi}\right)^{-1}\mathbf{Z}^{VSi}\right\}\right]\begin{bmatrix} \mathbf{J} \\ \mathbf{M} \end{bmatrix}=\begin{bmatrix} \mathbf{E}^{inc} \\ \mathbf{H}^{inc} \end{bmatrix}$$
$$(11)$$

with

$$\mathbf{Z}^{SSe}=\begin{bmatrix} \mathbf{Z}_{EJ}^{SSe} & \mathbf{Z}_{EM}^{SSe} \\ \mathbf{Z}_{HJ}^{SSe} & \mathbf{Z}_{HM}^{SSe} \end{bmatrix}, \quad (12)$$

$$\mathbf{Z}^{SSi}=\begin{bmatrix} \mathbf{Z}_{EJ}^{SSi} & \mathbf{Z}_{EM}^{SSi} \\ \mathbf{Z}_{HJ}^{SSi} & \mathbf{Z}_{HM}^{SSi} \end{bmatrix}, \quad (13)$$

$$\mathbf{Z}^{SVi}=\begin{bmatrix} \mathbf{Z}_{EJ}^{SVi} \\ \mathbf{Z}_{HJ}^{SVi} \end{bmatrix}, \quad (14)$$

$$\mathbf{Z}^{VSi}=\begin{bmatrix} \mathbf{Z}_{EJ}^{VSi} & \mathbf{Z}_{EM}^{VSi} \end{bmatrix}. \quad (15)$$

Note, that the matrix term in curly braces:

$$\mathbf{Z}_M=\left\{\mathbf{Z}^{SSi}-\mathbf{Z}^{SVi}\left(\mathbf{Z}_{EJ}^{VVi}\right)^{-1}\mathbf{Z}^{VSi}\right\} \quad (16)$$

may be calculated independently on the outer environment and/or excitation. Thus, once $\mathbf{Z}_M$ is obtained, the final system to be solved is that incorporating only surface sources with associated unknown coefficients. Taking into account that the number of unknowns associated with surface sources is usually many times smaller, than the number of unknowns corresponding to volume sources, solving (11) is much quicker that solving the original equation (3). Also, pre-calculated and stored $\mathbf{Z}_M$ may be re-used several times for different situations, and even for single problem incorporating cloning of the structure (like in analysis of antenna arrays, or other periodic geometries). The usefulness of above procedure was proven in [15], where pre-calculated $\mathbf{Z}_M$ was applied to analysis of Luneburg lenses for various types of excitations.

2.3 Integral-Equation Macromodel (IEM) of Luneburg Lens

The drawback of the domain decomposition technique outlined above is that the whole procedure must be repeated for every frequency of interest. One solution is to perform the computation at certain sample frequencies and then apply matrix interpolation [17] to $\mathbf{Z}_M$ for other frequencies. However, this matrix represents the partial problem solution, and therefore the elements of $\mathbf{Z}_M$ may exhibit resonant behavior (cf. [17]) leading to large numbers of frequency points to be analyzed directly, contrary to standard MoM techniques, where matrix elements represent simple source-field interactions. Therefore, in this work we make use of integral equation macromodels [10]. This technique, introduced previously by the author, allows to get the wideband approximation for $\mathbf{Z}_M$ making use of asymptotic waveform evaluation (AWE) technique (cf. [18]). The procedure consists of the following steps (cf. [10], [11]):

1. We find Taylor approximation to $\left(\mathbf{Z}_{EJ}^{VVi}\right)^{-1}\mathbf{Z}^{VSi}$ term, present in (16). The procedure relies on applying AWE method to the matrix equation:

$$\mathbf{Z}_{EJ}^{VVi} \cdot \mathbf{X} = \mathbf{U}, \tag{17}$$

vector $\mathbf{U}$ standing for successive columns of $\mathbf{Z}^{VSi}$. Note that we don't need to find the approximation to $\left(\mathbf{Z}_{EJ}^{VVi}\right)^{-1}$. The procedure has to be repeated only the number of times equal to the number of unknowns on the surface interface S, corresponding to the number of columns in $\mathbf{Z}^{VSi}$. This may be understood as exciting the structure by a limited number of "ports" at the interface.

2. Next, we obtain the Taylor coefficients of $\mathbf{Z}_M$ equating corresponding powers of left and right hand side expansions of (16).

3. Finally, we get Padé approximation for each element of $\mathbf{Z}_M$ utilising a usual procedure [18]. This final approximation, which is valid over some frequency interval, we call here the Integral Equation Macromodel (IEM) [10].

As seen above, the AWE method, and what follows integral equation macromodel technique, is based on Taylor expansions, which require computing of derivatives of the integral equation kernels, with respect to frequency. Luckily, here all kernels in (5) – (7) are the free-space ones, so the computation does not present difficulties. Proper formulas needed to compute derivatives of the kernels associated with surface sources may be found in [18]. The situation is a little bit more complicated for the case of kernels associated with volume sources, as the polarization current definition (2) itself includes the dependence on the frequency. Thus, we have to take it into account while computing the derivatives of proper matrix elements. The formulas for derivatives found in expressions for electric field due to polarization current may be found in author's paper [19], while the remaining formula for n-th derivative of the magnetic field kernel, multiplied by k, is:

$$\left(k(1+jkR)\frac{e^{-jkR}}{R^3}\right)^{(n)} =$$
$$\left\{kR(2n-1)+j\left[n(n-2)-k^2R^2\right]\right\}(-jR)^{n-2}\frac{e^{-jkR}}{R^2}. \tag{18}$$

Having the approximation to $\mathbf{Z}_M$, we compute both the sub-matrix of external interactions $\mathbf{Z}^{SSe}$ and the excitation vectors $\mathbf{E}^{inc}$, $\mathbf{H}^{inc}$, for a frequency of interest, and then solve (11), which is much quicker than solving original VIE. We can also introduce other objects external to S, which changes (11) into a larger linear set incorporating additional matrix blocks corresponding to interactions between the object and the surface S. This however does not change $\mathbf{Z}_M$ allowing it to be computed once and reused for different outer environments, excitation mechanisms and possible objects. As

mentioned in the Introduction, the first check of the above procedure was described in [11], where simple case of two-layer dielectric sphere was analyzed. Here, we present application of the method to more demanding case of Luneburg lenses.

3. Sample Results

First, we have applied the algorithm to model Luneburg lenses with moderate sizes ka ranging fro 5 to 20, where a is the lens radius. We have applied two BoR models: VIE model with the resolution 30×60 (see [9]) and VIE-SIE macromodel obtained with the same resolution for VIE part, and outer surface with radius $b = 1.5\,a$, with BoR generating arc divided into 150 segments. The geometrical details of basis functions used in the BoR model are those presented in author's earlier paper [16]. The quantity of interest was bistatic radar cross section (RCS) of the Luneburg lens.
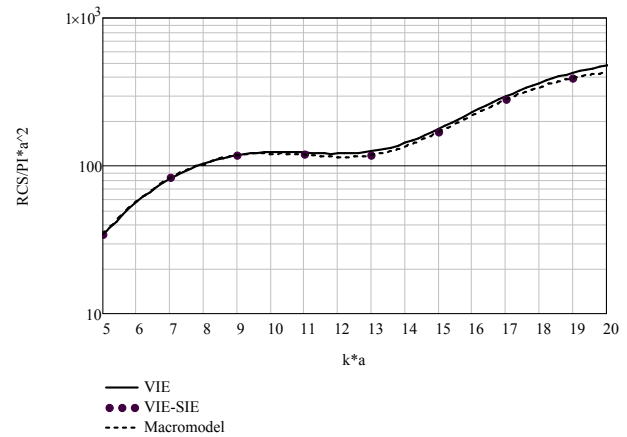

Fig. 3. Normalized forward RCS of the Luneburg lens – comparison of results.

The expansion points of the macromodel were values of $ka = 5, 7, 9, 11, 13, 15, 17$ and 19. The validity intervals associated with each expansion point were chosen to start and end in the midpoints between the expansion points, for instance for the interval from $ka = 6$ to 8, the computations were done using approximation obtained for the expansion point $ka = 7$. In the computations, orders of numerator and denominator of Padé approximations were $L = 5$ and $M = 5$, respectively.

In Fig. 3, it is shown the dependence of forward RCS with respect to electrical size of the lens. It is to be noted that the macromodel solution gives exact VIE-SIE values at the expansion frequencies of the macromodel, so those values, shown with black circles, allow to judge the exactness of the encapsulation of the lens with the additional surface, without involving wideband AWE approximations. From the figure, it is seen that the macromodel solution by definition ideally agrees with VIE-SIE solution at the expansion points. The agreement with the original VIE model for higher frequencies is less favorable.

Let's confine our interest to the *ka* interval from 5 to 10, where the agreement between VIE and VIE-SIE (and macromodel) solution seems almost ideal. Questions that arise are: whether it is possible to use a single expansion point to construct macromodels valid in the whole range, and what should be the order of Padé approximations in the macromodel construction. To answer those questions we performed calculations for the specified *ka* interval, choosing as the expansion point the mid value $ka = 7.5$, and applying different values of L and M, assuming however (see [18]) that $L = M$. The results are shown in Fig. 4.
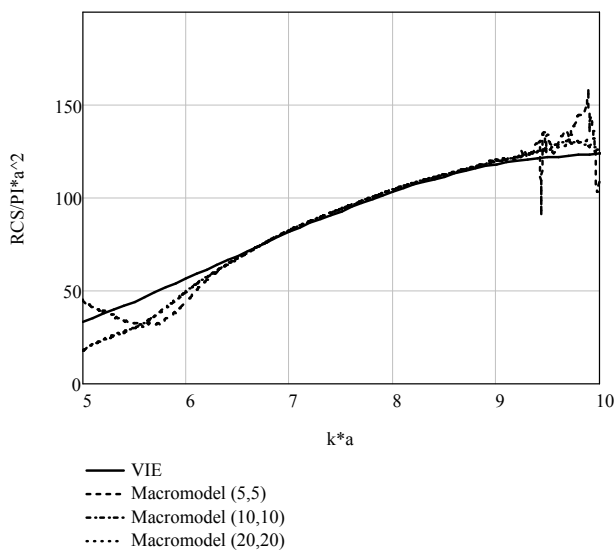

Fig. 4. Normalized forward RCS of the Luneburg lens – results for different macromodel orders.

One can see that in general increasing the order of approximation does not dramatically improve the frequency range of the macromodel. For the expansion point at $ka = 7.5$ we can judge the validity interval as ranging from $ka = 6.5$ to 9.0. This is however based on Fig. 4, which shows only forward RCS, not complete pattern. Therefore it is useful to compare also full bistatic RCS patterns at chosen frequencies. We performed comparisons for $ka = 6.5; 7.0; 7.5; 8.0; 8.5$ and 9.0. All plots denoted as "macromodel" were obtained using macromodels constructed around $ka = 7.5$. Results are shown in Fig. 5. From the figure it can be seen that real range of validity of the macromodel is from $ka = 7.0$ to 8.0. Increasing of the approximation order also in this case does not improve the quality of the macromodel. Thus, we may draw the conclusion that it is better to use more expansion points and lower orders of approximations.

The main purpose of the "black-boxing" the Luneburg lens was to decrease the number of unknowns in the final solution. In the above examples, this corresponds to the reduction of the set of 3630 linear equations (original VIE) to 598 linear equations (number of unknowns in (11)). Thus, in the example, we reduced the number of unknowns about six times. In direct solvers, using for example Gaussian elimi-

nation or lower-upper-triangular decomposition, the number of operations is proportional to $O(N^3)$ [18], where N is the number of unknowns. So, the six-times reduction of N is equivalent to more than 200 times reduction of the number of operations, at the stage of final solution of the linear equation set.

Of course, we do not count here the time needed for the macromodel construction, but the original idea of integral equation macromodels lies in the possibility of reusing once constructed macromodel in several different configurations/environments [10].

4. Conclusions

In this paper we have applied integral equation macromodels to speed-up calculations involving modeling of Luneburg lenses. It has been shown that although resulting macromodels are not very wideband, it still makes sense to apply them for more efficient integral-equation/method-of–moments analyzes. Once a macromodel is constructed for a given frequency interval, the computation time needed for solving the final system of equations may be considerably reduced. The constructed macromodel remains within the BoR scheme, this is however not the limitation, in view of the existence of convenient scheme enabling the analysis of mixed BoR-3D geometries with the use of so-called characteristic basis functions (CBFs) [20].

References

[1] LUNEBURG, R. K., HERZBERGER, M. *The Mathematical Theory of Optics*. Providence (RI, USA): Brown University Press, 1944.

[2] GREENWOOD, A. D., JIN, J.-M. A field picture of wave propagation in inhomogeneous dielectric lenses. *IEEE Antennas and Propagation Magazine*, 1999, vol. 41, no. 5, p. 9 - 18.

[3] MOSALLAEI, H., RAHMAT-SAMII, Y. Nonuniform Luneburg and two-shell lens antennas: Radiation characteristics and design optimization. *IEEE Transactions on Antennas and Propagation*, 2001, vol. 49, no. 1, p. 60 - 69.

[4] LIANG, C. S., STREATER, D. A., JIN, J.-M., DUNN, E., ROZENDAL, T. A quantitative study of Luneburg-lens reflectors. *IEEE Antennas and Propagation Magazine*, 2005, vol. 47, no. 7, p. 30 - 41.

[5] THORNTON, J. Properties of spherical lens antennas for High Altitude Platform communications. In *6th European Workshop on Mobile/Personal Satcoms & 2nd Advanced Satellite Mobile Systems (EMPS & ASMS)*. 2004.

[6] THORNTON, J. Wide-scanning multi-layer hemisphere lens antenna for Ka band. *IEE Proceedings – Microwaves, Antennas and Propagation*, 2006, vol. 153, no. 6, p. 573 - 578.

[7] MORGAN, M. A., MEI, K. K., Finite-element computation of scattering by inhomogeneous penetrable bodies of revolution. *IEEE Transactions on Antennas and Propagation*, 1979, vol. 27, no. 2, p. 202 - 214.

[8] GREENWOOD, A. D., JIN, J.-M. A novel, efficient algorithm for scattering from a complex BOR using mixed finite elements and
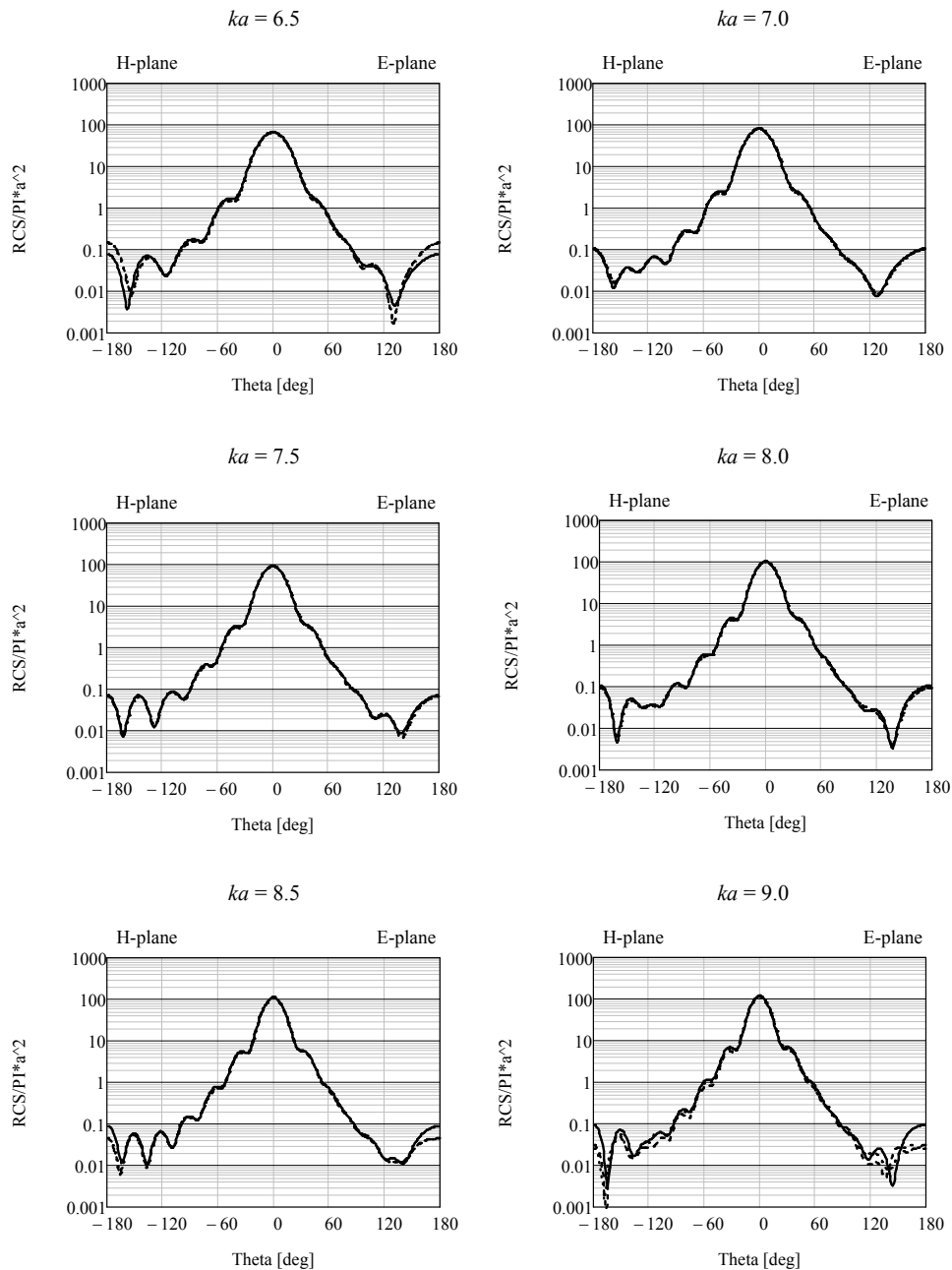
Fig. 5. Bistatic RCS of the Luneburg lens computed using VIE (solid lines), macromodel with $L = 5$, $M = 5$ (dashed lines), and macromodel with $L = 10$, $M = 10$ (dotted lines).

cylindrical PML. *IEEE Transactions on Antennas and Propagation*, 1999, vol. 47, no. 4, p. 620 - 629.

[9] KUCHARSKI, A. A. A method of moments solution for electromagnetic scattering by inhomogeneous dielectric bodies of revolution. *IEEE Transactions on Antennas and Propagation*, 2000, vol. 48, no. 8, p. 1202 - 1210.

[10] KUCHARSKI, A. A. Efficient solution of integral-equation based electromagnetic problems with the use of macromodels. *IEEE Transactions on Antennas and Propagation*, 2008, vol. 56, no. 5, p. 1482 - 1487.

[11] KUCHARSKI, A. A. Wideband analysis of electromagnetic scattering from partially inhomogeneous dielectric bodies-of-revolution with the use of macromodels. In *3rd European Conference on Antennas and Propagation (EuCAP)* Berlin (Germany), 2009, p. 93 - 96.

[12] HARRINGTON, R. F. *Time-Harmonic Electromagnetic Fields*. McGraw-Hill Book Company, 1961.

[13] SCHAUBERT, D. H., WILTON, D. R., GLISSON, A. W. A tetrahedral modeling method for electromagnetic scattering by arbitrarily shaped inhomogeneous dielectric bodies. *IEEE Transactions on Antennas and Propagation*, 1984, vol. 32, no. 1, p. 77 - 85.

[14] LI, M.-K., CHEW, W. C., JIANG, L. J. A domain decomposition scheme based on equivalence theorem. *Microwave and Optical Technology Letters*, 2006, vol. 48, no. 9, p. 1853 - 1857.

[15] KUCHARSKI, A. A. Analysis of Luneburg lenses using domain decomposition method. In *17th International Conference on Microwaves, Radar and Wireless Communications (MIKON)*. 2008.

[16] KUCHARSKI, A. A. Electromagnetic scattering by partially inhomogeneous dielectric bodies of revolution. *Microwave and Optical Technology Letters*, 2005, vol. 44, no. 3, p. 275 - 281.

[17] NEWMAN, E. H. Generation of wide-band data from the method of moments by interpolating the impedance matrix. *IEEE Transactions on Antennas and Propagation*, 1988, vol. 36, no. 12, p. 1820 - 1824.

[18] CHEW, W. C., MICHIELSSEN, E., SONG, J. M., JIN, J. M. *Fast and Efficient Algorithms in Computational Electromagnetics*. Boston, London: Artech House, 2001.

[19] KUCHARSKI, A. A. Asymptotic waveform evaluation for scattering by inhomogeneous dielectric bodies of revolution, *Microwave and Optical Technology Letters*, 2007, vol. 49, no. 5, p. 1028 - 1031.

[20] KUCHARSKI, A. A. Application of the CBF method to the scattering by combinations of bodies of revolution and arbitrarily shaped structures. *Radioengineering*, 2013, vol. 22, no. 3, p. 665 - 671.

About Author . . .

Andrzej A. KUCHARSKI was born in 1964. He received his M.Sc., Ph.D. and D.Sc. from Wroclaw University of Technology in 1988, 1994, and 2001, respectively. He is the Head of the Antenna Theory and Computational Electromagnetics Group in the Telecommunications and Teleinformatics Department, Faculty of Electronics, Wroclaw University of Technology, Poland. His research interests include computational electromagnetics in radiation and scattering problems.